Real-Time Coordinated Voltage Control of PV Inverters and Energy Storage for Weak Networks with High PV Penetration

Licheng Wang, *Student Member, IEEE*, Feifei Bai, *Member, IEEE*, Ruifeng Yan, *Member, IEEE*, Tapan Kumar Saha, *Senior Member, IEEE*

***Abstract*—There are more large-scale PV plants being established in rural areas due to availability of low priced land. However, distribution grids in such areas traditionally have feeders with low X/R ratios, which makes the independent reactive power compensation method less effective on voltage regulation. Consequently, upstream Step Voltage Regulator (SVR) may suffer from excessive tap operations with PV induced fast voltage fluctuations. Although a battery energy storage system (BESS) can successfully smooth PV generation, frequent charge/discharge will substantially affect its cost effectiveness. In this paper, a real-time method is designed to coordinate PV inverters and BESS for voltage regulation. To keep up with fast fluctuations of PV power, this method will be executed in each 5s control cycle. In addition, charging/discharging power of BESS is adaptively retuned by an active adjustment method in order to avoid BESS premature energy exhaustion in a long run. Finally, through a voltage margin control scheme, the upstream SVR and downstream PV inverters and BESS are coordinated for voltage regulation without any communication. This research is validated via an RTDS-MatLab co-simulation platform, and it will provide valuable insights and applicable strategies to both utilities and PV owners for large-scale PV farm integration into rural networks.**

***Index Terms*-- Coordinated voltage control, photovoltaic (PV), battery energy storage system (BESS), real-time control, state of charge (SOC) regulation.**

I. Introduction

With rapid development of photovoltaic (PV) technology, more large-scale PV systems are being integrated into rural areas where abundant solar energy and low-cost land are readily available. However, distribution networks in these areas are usually weak in nature due to their remoteness. Therefore, voltage violation issues [1, 2] caused by PV variability arise when PV penetration becomes substantially high.

Currently, voltage regulation in distribution systems mainly relies on traditional devices such as step voltage regulators (SVR) and on-load tap-changer (OLTC) transformers, which are mainly designed to compensate a slow changing voltage due to load variations. However, with the increase of PV penetration, the voltage variability becomes much more significant. Therefore, traditional voltage regulators may not be sufficient to control the rapid voltage variations caused by fluctuations of renewable energy generation [3], especially in remote networks [4]. In this situation, reactive power compensation through PV inverters is first proposed to improve the voltage profile due to their availability and low cost [5-8]. However, with low X/R ratio of rural distribution systems, reactive power compensation methods for voltage regulation are not as effective as those in transmission systems. In addition, the reactive power of PV inverters is generally limited by the power factor restriction (e.g. between 0.9 lagging to 0.9 leading) based on the Connection Agreement [9], which further weakens its voltage regulation ability. Hence, a battery energy storage system (BESS) is proposed to support PV systems with charging/discharging operations [10-12]. Although the widely implemented moving average algorithm [13] for BESS can effectively improve voltage profile through smoothing PV power output, the resultant frequent charging/discharging operations can decrease the BESS life span, which makes the BESS solution uneconomical. In addition, most of the current studies rely on a BESS with a relatively large size, which is not always available in real-life application, and realistic limits (e.g. ramp rate, inverter capacity and power factor range) are usually neglected during controller design.

Considering disadvantages of the above independent control schemes, recent development manages to coordinate various devices in voltage regulation, aiming to successfully control system voltage with less cost. For example, in [14-18], operation points of different devices (e.g. inverters, batteries, OLTC) are adjusted in each control cycle by coordinated methods for voltage regulation. The control cycle selected in these coordinated methods is usually in a time scale of a few minutes to one hour, which may be effective with slowly changing PV power in clear sky days. However, the generation of a mega-watt scale PV plant may drop more than 70% of its rated capacity in a couple of minutes due to fast moving clouds. Therefore, these non-real-time methods may not be suitable under cloudy weather conditions.

In this paper, a new real-time coordinated voltage control method is developed and verified on the Real Time Digital Simulator (RTDS) [19] with the field recorded PV and load data. The main contributions of this paper are summarized as follows:

1) Real-time voltage regulation scheme. In order to keep up with the fast fluctuations of PV power, a real-time method based on short-term voltage sensitivity control is proposed to coordinate PV inverters and BESS for

Corresponding author Ruifeng Yan is with the School of Information Technology and Electrical Engineering, The University of Queensland, Brisbane, QLD 4072, Australia (e-mail: ruifeng@itee.uq.edu.au).

Licheng Wang, Feifei Bai and Tapan Kumar Saha are with the School of Information Technology and Electrical Engineering, The University of Queensland, Brisbane, QLD 4072, Australia (e-mail: l.wang8@uq.edu.au, f.bai@uq.edu.au, saha@itee.uq.edu.au).

voltage regulation. A variety of techno-economic aspects have been taken into consideration, such as minimization of BESS usage, limited ramp rate and power factor range, restrained BESS capacity and inverter size.

2) Coordination between remote SVR and PV inverters-BESS without the need of communication. In addition to the proposed short-term voltage sensitivity based approach for real time voltage regulation, a new long-term voltage margin control scheme is developed for the coordination between the upstream step voltage regulator (SVR) and the downstream PV-BESS system without any communication. Under such a design, PV inverters and BESS are mainly used to counter voltage variations caused by fast fluctuating PV power; while the SVR is responsible for compensating the long-term voltage variation tendency which is mainly caused by slowly changing load demand and upstream voltage profile.
3) BESS state of charge (BESS) regulation. With real-time measurements, the voltage control method developed so far mainly focuses on the optimal voltage regulation in each control cycle, which may lead to premature energy exhaustion of the BESS due to its limited capacity. Therefore, an active adjustment method is proposed to adaptively retune the charging/discharging power of BESS in each control cycle for state of charge (SOC) regulation. This is to overcome the short sight of the real-time method. Therefore, BESS can be mostly available for voltage regulation when required.

Simulation results with a RTDS-MatLab co-simulation platform are demonstrated in this paper to verify the effectiveness of the proposed method in real-time application. With this proposed method, excessive voltage violations, SVR tap operations and battery usage are successfully mitigated.

II. Background Description

The system studied in this paper is a typical example of a large-scale PV installation into the fringe of the grid – a 3.275MWp PV plant with (600kW, 760kWh) BESS located at the University of Queensland (UQ) Gatton campus. The campus has a general loading range of 1.5-3MW during the daytime, so the instantaneous penetration level can be as high as 200% under low load conditions.

As shown in Fig. 1, this PV plant is connected to the Gatton zone substation through an 11kV 7.45km long feeder, where an SVR with open-delta connection is installed in the middle for downstream voltage regulation. The details of the SVR and its tap switching mechanism are presented in Appendix A. Campus load, PV arrays and BESS are connected to the 11kV distribution feeder through 11kV/415V transformers with delta-grounded wye connection.

Fig. 2 is a schematic figure, which describes how the studied PV arrays, BESS and their corresponding communication system are connected in the UQ Gatton campus. All inverters are controlled by programmable logic controllers (PLCs), through which real-time field recorded measurements can be read and transmitted to the supervisory control and data acquisition (SCADA) system every one second. At the same time, PLC will update operation points of inverters every one second according to the control commands issued by the SCADA.

Currently, the PV inverters provide reactive power compensation following a power factor droop curve [20], and the BESS controls its charging/discharging operations with a 5-minute moving average algorithm [13]. The detail of the power factor droop curve and moving average algorithm can be found in Appendices B and C, respectively.

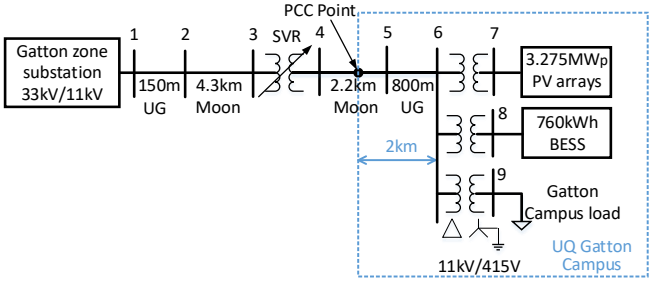

Fig. 1 Single line diagram of the UQ Gatton distribution network.

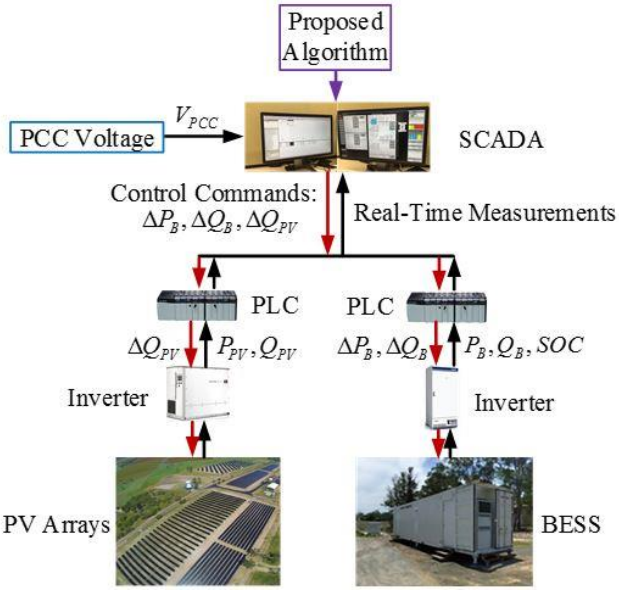

Fig. 2 System structure and information flows.

The Gatton 11kV distribution feeder has a relatively low X/R ratio of around 1.18, which limits the influence of reactive power support on voltage control. Moreover, the voltage regulation ability is further weakened by the power factor boundaries (between 0.9 lagging to 0.9 leading) according to the Connection Agreement [9]. Especially when PV generation quickly drops to a very low level as a result of cloud coverage, PV inverters should increase reactive power injection to compensate the corresponding voltage drop. However, due to the power factor limit, PV inverters have to reduce their reactive power output with dropping active generation. Therefore, reactive power compensation alone may not totally mitigate voltage variations caused by strong PV power fluctuations in the weak Gatton network. As a result, consequent issues that should be addressed are summarized as follows.

A. Voltage Violation

According to the Connection Agreement [9] between UQ and the local utility, the line-to-line voltage at the point of common coupling (PCC) should always be maintained within [0.975 pu to 1.01 pu]. Otherwise, the PV owner (UQ)

can be penalized due to voltage violation. With the current independent voltage control scheme via different regulation devices, voltage violation can be observed, especially on cloudy days.

B. Excessive Tap Operation of SVR

With limited ability of reactive power compensation in voltage regulation, large voltage variations at PCC cannot be successfully mitigated especially on cloudy days. As a result, tap operations of the upstream SVR will be frequently triggered to counter downstream voltage fluctuations, and such excessive tap operations will lead to a shorter life span and higher maintenance of the SVR.

C. Overuse of BESS

BESS is one kind of effective but expensive resource for voltage regulation. Following the widely implemented moving average algorithm with a long window length T (detail is shown in Appendix C), PV power can be successfully smoothed. As a result, voltage violations and excessive SVR tap operations can be effectively mitigated at the same time. However, BESS will be overused, especially on cloudy days. For example, with a 10-minute window length of the moving average algorithm, the 760kWh BESS would process 5290kWh energy (around 7 times of its rated capacity) on a typical cloudy day. It should be noted that in this paper the BESS usage is evaluated by its total processed energy, which is also known as the wear level of BESS [21].

III. PV Power Prediction for Real-Time Voltage Control Scheme

To successfully manage system voltage with lower cost (fewer SVR tap operations and less total processed energy of BESS), a real-time voltage regulation method will be proposed in Section IV to optimally coordinate PV inverters and BESS for voltage regulation. As designed, the real-time voltage control scheme is mainly used to offset short-term voltage variations caused by fast PV power fluctuations. Once PV induced voltage fluctuations are mitigated, the SVR will consequently be left to deal with slow load changes and upstream voltage variations. Therefore, the volume of voltage variation that needs to be compensated by PV inverters and BESS through the real-time voltage control scheme in each control cycle should be estimated. In this section, the characteristic of PV power fluctuations will be demonstrated first. On this basis, a very short term PV power prediction with real-time measurements as well as control cycle design are presented.

A. Fluctuation Characteristic of PV Power

The characteristic of PV power fluctuations is different in different time scales, which has a significant impact on the design of voltage regulation. As shown in Fig. 3, PV generation will experience frequent fluctuations during a typical cloudy day, and PV power shows a high level of variability in a time scale of minutes to hours. However, PV power variations manifest an approximately linear tendency in the time scale of seconds, as shown in the zoom-in picture of Fig. 3. This is due to the fact that it takes the fast-moving cloud a few minutes to totally cover a PV plant with a dimension of $700m \times 300m$. Therefore, within a short time period, PV power can be adequately predicted through linear estimation.

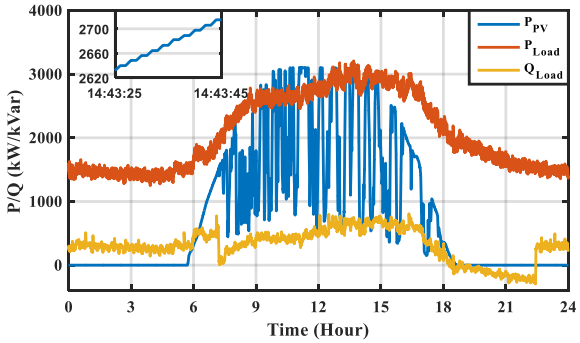

Fig. 3 PV power fluctuations in different time scales.

B. PV Power Prediction and Control Cycle Design

Based on the analysis of PV power fluctuations in different time scales, a 5s control cycle is selected in this paper. Because optimal adjustments obtained in each 5s control cycle is fast enough to follow the power fluctuations of a PV plant, and accurate PV power prediction can be attained through a leaner forecast model. As shown in Fig. 4, PV power will be measured twice in each control cycle at time instants t and $t+2$. Based on these two measurements, the PV generation at time instant $t+5$ is estimated through a linear forecast model [22] as

$$\tilde{P}_{PV}(t+5) = P_{PV}(t) + \frac{5s}{2s}[P_{PV}(t+2) - P_{PV}(t)] \quad (1)$$

where $\tilde{P}_{PV}(t+5)$ represents the predicted PV generation at time instant $t+5$; $P_{PV}(t)$ represents the measured PV generation at time instant t. Therefore, the corresponding voltage deviation ΔV_{PV} caused by PV power variation in each 5s control cycle can be estimated as

$$\Delta V_{PV} = \frac{\partial V}{\partial P}[\tilde{P}_{PV}(t+5) - P_{PV}(t)] \quad (2)$$

where $\frac{\partial V}{\partial P}$ represents the average line-to-line voltage (V_{AB}, V_{BC}, V_{CA}) sensitivity at PCC with respect to active power injection at the PV connection point.

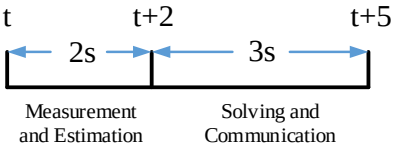

Fig. 4 A 5 second control cycle.

IV. Proposed Method for Coordinated Voltage Control

As shown in Fig. 5, the proposed method which is executed in each control cycle is composed of two parts, namely the optimization algorithm and the active adjustment method. The optimization algorithm is responsible for real-time voltage regulation (voltage smoothing, voltage violation correction); while the active adjustment method is responsible for BESS SOC regulation. The inputs of the proposed method are real-time measurements including active power of battery P_B, reactive power of battery Q_B, battery SOC, active power of PV inverters P_{PV}, reactive

power of PV inverters Q_{PV} and PCC voltage V_{PCC}. With these measurements, the proposed method sends control commands (active and reactive power variations ΔP_B, ΔQ_B and ΔQ_{PV}) to BESS and PV inverters in each control cycle. The optimization algorithm for real-time voltage regulation will be introduced in this section, and the detail of the active adjustment method for SOC regulation will be provided in Section V.

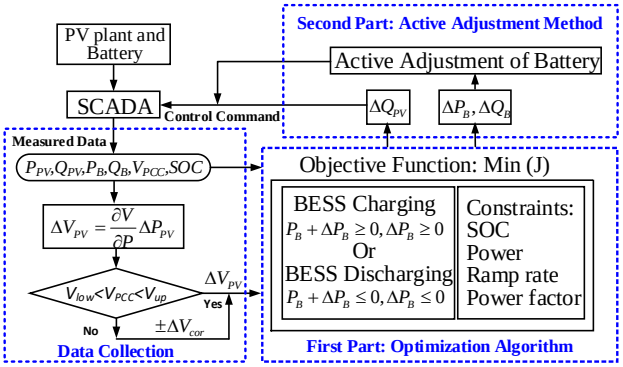

Fig. 5 Flow chart of the proposed method in each control cycle.

A. Voltage Smoothing

PV inverters and BESS are coordinated in the proposed method to compensate voltage variations ΔV_{PV} caused only by PV power fluctuations in each control cycle. As designed, reactive power compensation always has a priority to be used in voltage regulation in order to mitigate the usage of BESS. Therefore, the objective function can be formulated as

$$J = \underbrace{\left|\Delta V_{PV} + \frac{\partial V}{\partial P}\Delta P_B + \frac{\partial V}{\partial Q}(\Delta Q_B + \Delta Q_{PV})\right|}_{voltage\ variation} + \alpha \underbrace{|P_B + \Delta P_B|}_{power\ of\ BESS} \quad (3)$$

where ΔV_{PV} is estimated by (2); $\frac{\partial V}{\partial Q}$ represents the average line-to-line voltage sensitivity at PCC with respect to reactive power injection; For the current system topology, parameters $\frac{\partial V}{\partial P}$ and $\frac{\partial V}{\partial Q}$ are $1.34 \times 10^{-5} pu/kW$ and $1.54 \times 10^{-5} pu/kVar$ respectively; ΔP_B , ΔQ_B and ΔQ_{PV} are variables to be optimized. The first part of (3) represents the voltage variation, and the second part of (3) is the charging/discharging power of BESS and α is a weight factor with a small positive value. Hence, the objective function will first highlight voltage smoothing, namely minimizing the first part of (3). Only when reactive power support alone (ΔQ_B and ΔQ_{PV}) can totally compensate ΔV_{PV} (the first part is zero), the objective function will then try to minimize $|P_B + \Delta P_B|$ for saving the BESS usage. With mitigated voltage fluctuations at PCC, the system voltage can be successfully regulated by upstream SVR with a few tap operations per day.

B. Voltage Correction

Once a voltage violation risk is detected, ΔV_{PV} in the object function will be adjusted as in (4). Therefore, the function of the real-time voltage regulation scheme is changed from voltage profile smoothing to voltage correction.

$$\Delta V_{PV}^{m} = \begin{cases} \Delta V_{PV} + \Delta V_{cor}, & if\ V_{PCC} > V_{up} \\ \Delta V_{PV} - \Delta V_{cor}, & if\ V_{PCC} < V_{low} \end{cases} \quad (4)$$

where ΔV_{PV}^{m} represents the modified value of ΔV_{PV} ; $[V_{low}, V_{up}]$ is a voltage range which is set to be [0.978 pu, 0.997 pu] in this paper. As in (4), the voltage correction function will be triggered if the measured PCC voltage is out of the range $[V_{low}, V_{up}]$.

A detail example is demonstrated as in Fig. 6 to explain the voltage margin control scheme which coordinates the upstream SVR and the downstream BESS and PV inverters, when a long-term voltage violation risk occurs. As in Fig. 6, V_t and ΔV_{db} represents the voltage target and dead band of SVR respectively; 0.975pu is the lower voltage limit of the point of common coupling (PCC) according to the Connection Agreement [9]. When voltage at PCC drops to less than $V_t - \Delta V_{db}$, the timer of SVR begins to count, and an SVR tap lift is expected if this low voltage can last longer than its time delay (135s). In addition, if the voltage continuously falls below V_{low} before the SVR tap operation as illustrated in Fig. 6 (time instant t_1), the voltage correction function in the real-time voltage regulation scheme will be triggered, and an extra voltage correction ΔV_{cor} will be added in the voltage compensation target as in (4). As a result, PV inverters and BESS will adjust their output to lift the PCC voltage with a volume of ΔV_{cor}. If the selected voltage correction volume ΔV_{cor} is too large, the PCC voltage after correction may be larger than $V_t - \Delta V_{db}$, which will interrupt the SVR timer, and no SVR tap operation is expected. Consequently, the system voltage has to be supported only by PV inverters and BESS for a long time. Hence, the BESS will be overused, and this is uneconomical in voltage regulation.

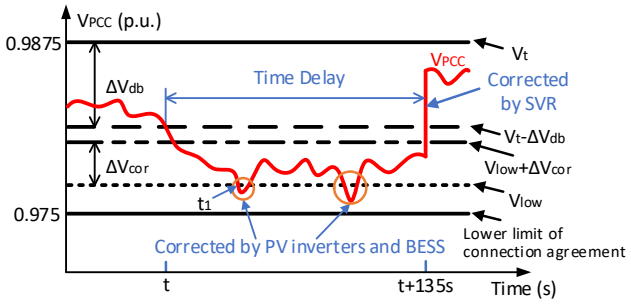

Fig. 6 Voltage margin control scheme.

In our proposed method, the voltage correction ΔV_{cor} in the real-time voltage regulation scheme should be satisfied with

$$V_{low} + \Delta V_{cor} < V_t - \Delta V_{db}$$

With such design, the PCC voltage after correction from the real-time voltage regulation scheme is still lower than $V_t - \Delta V_{db}$, and the timer of the SVR will not be interrupted. Therefore, system voltage will be lifted by one or more SVR tap operations after the low voltage lasts longer than the SVR time delay (135s). As a result, BESS and PV inverters can reduce their contribution in voltage compensation, and over usage of BESS can be avoided.

To sum up, the main task of PV inverters and BESS is to smooth the voltage variations caused by fast PV power fluctuations. While, PV inverters and BESS will also be temporarily involved in voltage correction when a voltage violation risk arises and the over-correction of voltage should be avoided. As a result, the upstream SVR is left to

compensate long-term and slowly changing voltage variations. Therefore, the proposed method can not only alleviate the voltage violation problem, but also mitigate excessive SVR tap operations and battery usage.

C. Constraints

a) *Ramp Rate Limit*

The ramp rate limits of active and reactive power of PV and BESS inverters in each control cycle are formulated as follows:

$$|\Delta Q_B| \le \Delta Q_{B,max} \cdot \Delta t \quad (5)$$

$$|\Delta P_B| \le \Delta P_{B,max} \cdot \Delta t \quad (6)$$

$$|\Delta Q_{PV}| \le \Delta Q_{PV,max} \cdot \Delta t \quad (7)$$

where Δt represents the time interval of a control cycle (5s). In Gatton PV plant, the ramp rate limits of ΔQ_B, ΔP_B and ΔQ_{PV} are 20kVar/s, 20kW/s and 50kVar/s, respectively.

b) *Power Limit*

Reactive power limits of inverters are not required due to the existing power factor limits. Therefore, only the maximum active power limit $P_{B,max}$ of BESS is included as

$$|P_B + \Delta P_B| \le P_{B,max} \quad (8)$$

c) *Battery Capacity Limit*

The SOC of the BESS should always remain within a given range in order to avoid BESS damage.

$$SOC_{min} \le SOC \le SOC_{max} \quad (9)$$

where SOC_{max} and SOC_{min} represent the upper and lower limits of the SOC of BESS.

d) *Power Factor Limit*

The power factor of PV inverters should not be lower than 0.9.

$$\frac{P_{PV}+\Delta P_{PV}}{\sqrt{(P_{PV}+\Delta P_{PV})^2+(Q_{PV}+\Delta Q_{PV})^2}} \ge 0.9 \quad (10)$$

(10) can be equivalently converted to a convex format as

$$-\sqrt{\frac{19}{81}}(P_{PV}+\Delta P_{PV}) \le Q_{PV}+\Delta Q_{PV} \le \sqrt{\frac{19}{81}}(P_{PV}+\Delta P_{PV}) \quad (11)$$

where $\sqrt{\frac{19}{81}} = \sqrt{\frac{(1-PF^2)}{PF^2}}$ with power factor PF equal to 0.9.

The power factor of battery inverters should conform to the same limits as well.

$$\frac{|P_B+\Delta P_B|}{\sqrt{(P_B+\Delta P_B)^2+(Q_B+\Delta Q_B)^2}} \ge 0.9 \quad (12)$$

To establish convex constraints, (12) can be split into two situations, namely regarding a battery as a load or regarding a battery as a generator. If the battery is charging (as a load), (12) can be equivalently converted into

$$\sqrt{\frac{19}{81}}(P_B+\Delta P_B) \le Q_B+\Delta Q_B \le \sqrt{\frac{19}{81}}(-P_B-\Delta P_B) \quad (13)$$

$$P_B + \Delta P_B \le 0 \quad (14)$$

Similarly, if the battery is discharging (as a generator), (12) can be equivalently converted into

$$-\sqrt{\frac{19}{81}}(P_B+\Delta P_B) \le Q_B+\Delta Q_B \le \sqrt{\frac{19}{81}}(P_B+\Delta P_B) \quad (15)$$

$$P_B + \Delta P_B \ge 0 \quad (16)$$

Overall, two optimization problems with assumptions of BESS as a load and a generator are demonstrated below.

Min (3)

Constraints: (5)~(9), (11), (13)~(14)

and

Min (3)

Constraints: (5)~(9), (11), (15)~(16)

These two optimization problems can be solved by CVX optimization tool box [23] separately within around 0.4s in total. The final optimal solution (ΔP_B, ΔQ_B and ΔQ_{PV}) can be obtained through comparing results of these two optimization problems (one of them may be infeasible).

D. Discussion on Voltage Sensitivity

Voltage sensitivities are used in above formulations to simplify the optimization problem which should be quickly solved in each 5s control cycle. However, voltage sensitivities with respect to active and reactive power injection are dependent on current system state. System state variations that influence voltage sensitivities can be classified into two groups:

1) Line power flow variation. With PV power fluctuations and load level variations, line power flow changes all the time. However, line power flow variation only has an insignificant impact on voltage sensitivities. For example in this paper, the voltage sensitivity deviation with respect to reactive power injection between high PV generation low load scenario and low PV generation high load scenario is within 3%. Furthermore, the voltage sensitivities have already been widely used to simplify formulations for distribution systems as in [7, 24, 25].
2) Distribution system reconfiguration. Distribution system reconfiguration will have a more significant impact on voltage sensitivities. However, the number of possible system reconfigurations is limited, and distribution system reconfiguration will not frequently occur. Therefore, a database should be established to store different voltage sensitivities corresponding to all possible system configurations [7]. Once the system is reconfigured, the voltage sensitivities used in the objective function should be correspondingly updated.

V. Active Adjustment Method for SOC Regulation

The optimization algorithm can be very effective, but it only focuses on the optimal dispatch for voltage regulation in each control cycle. Hence, with limited BESS capacity, the SOC of BESS in a long run may reach its upper or lower limit before the SOC can be gradually adjusted back to its ideal middle level during the night-time. As a result, BESS may become unavailable for voltage regulation when voltage violation risk arises. Therefore, an active adjustment method is required to adaptively retune ΔP_B and ΔQ_B (variations of BESS active and reactive power) obtained from the optimization algorithm in order to avoid premature BESS energy exhaustion.

The capacity of the installed 760kWh BESS in Gatton PV plant is relatively small compared with that of the

3.275MWp PV arrays. Moreover, in order to avoid damaging the BESS, the upper and lower limits of SOC are set to be 90% (684kWh) and 40% (304kWh), respectively. Therefore, only 380kWh is available for dispatch. In this situation, the designed active adjustment method for SOC regulation is indispensable.

A. Basic Idea for SOC Regulation

ΔP_B obtained from the optimization algorithm can be either positive or negative in a control cycle. For example, a positive ΔP_B means an increase of discharging power or a reduction of charging power of BESS. For the purpose of SOC regulation, the tunning rules of ΔP_B should have certain functionalities in the following aspects.

1) Direction of Adjustment. ΔP_B should be tuned to a larger value (denoted as ΔP_B^m – meaning ΔP_B after modification) if the current SOC is higher than its middle level SOC_{mid}. As a result, discharging power of BESS is increased (or charging power of BESS is reduced), which will prevent SOC from approaching its upper limit. Conversely, if SOC is lower than its middle level SOC_{mid}, ΔP_B should be reduced to avoid energy exhaustion. This functionality can be summarized as:

$$① \ \Delta P_B^m > \Delta P_B \ if \ SOC > SOC_{mid}$$

$$\text{and } \Delta P_B^m < \Delta P_B \ if \ SOC < SOC_{mid}$$

In addition, when current SOC level approaches to its lower limit SOC_{min}, ΔP_B^m should approach to zero if a positive ΔP_B is obtained from the optimization algorithm. This functionality can be present as below.

$$② \ SOC \to SOC_{min}^{+} \Rightarrow \Delta P_B^m \to 0^+$$

Similarly, with a negative ΔP_B obtained from the optimization algorithm, ΔP_B^m (charging) should be tuned to zero, if current SOC level approaches to its upper limit SOC_{max}.

2) Magnitude of Adjustment. The magnitude of active adjustment should depend on the distance between current SOC level and its middle level SOC_{mid}. If the current SOC level is far away from its middle level SOC_{mid}, a stronger adjustment is preferred to bring the SOC back to the middle level. While, if the current SOC is equal to SOC_{mid}, the effect of active adjustment becomes zero. These functionalities can be summarized as below:

$$③ \ |\Delta P_B^m - \Delta P_B| \begin{cases} \text{monotonically increases}, SOC > SOC_{mid} \\ \text{monotonically decreases}, SOC < SOC_{mid} \end{cases}$$

and

$$④ \ SOC \to SOC_{mid} \Rightarrow \Delta P_B^m \to \Delta P_B$$

The SOC regulation functionalities discussed above are illustrated as in Fig. 7 for situations with either positive or negative ΔP_B.

It is worth noting that the active adjustment method will not be executed when a voltage violation risk is detected. Therefore, the voltage violation correction function of the proposed method will not be compromised when there is a strong need of voltage regulation.

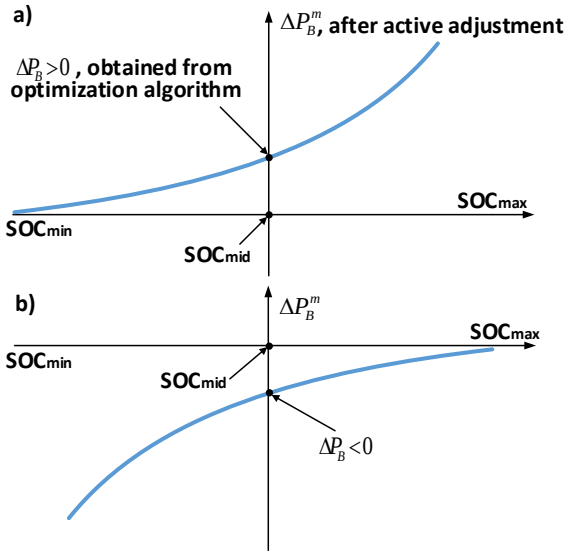

Fig. 7 a) Active adjustment of BESS power when ΔP_B is positive; b) Active adjustment of BESS power when ΔP_B is negative

B. Formulation

The active adjustment method can be designed as (17) to fulfil the required functionalities presented in Part A of this section.

$$\Delta P_B^m = \begin{cases} \Delta P_B e^{\frac{c_2(SOC-SOC_{mid})}{SOC-SOC_{min}}}, & if \ \Delta P_B > 0, fl = 0 \\ \Delta P_B e^{\frac{c_2(SOC_{mid}-SOC)}{SOC_{max}-SOC}}, & if \ \Delta P_B < 0, fl = 0 \end{cases} \quad (17)$$

where $fl = 0$ indicates the situation when no voltage violation risk is detected; c_2 is a positive constant, which is used to adjust the slope of the exponential curve; In this paper, c_2 is set to be 2. It is worth noting that (17) is different from the hard boundary constraint (9) included in the optimization algorithm, which will not be effective until SOC reaches its upper or lower limit. Instead, (17) is a soft constraint, which works with all possible SOC levels. Proof of the effectiveness of the designed active adjustment method in SOC regulation is provided in Appendix D.

Finally, in order to always respect the power factor restriction (0.9 leading to 0.9 lagging according to the Connection Agreement), the reactive power generation of BESS should be checked and correspondingly modified as in (18) after the adjustment of active power of BESS.

$$Q_B^m = \begin{cases} Q_B + \Delta Q_B, & if \ |Q_B + \Delta Q_B| < (P_B + \Delta P_B^m)\sqrt{\frac{19}{81}} \\ (P_B + \Delta P_B^m)\sqrt{\frac{19}{81}}, & if \ Q_B + \Delta Q_B > (P_B + \Delta P_B^m)\sqrt{\frac{19}{81}} \\ -(P_B + \Delta P_B^m)\sqrt{\frac{19}{81}}, & if \ Q_B + \Delta Q_B < -(P_B + \Delta P_B^m)\sqrt{\frac{19}{81}} \end{cases} \quad (18)$$

VI. Additional Challenges with Proposed Method

Compared with the existing local control schemes, the additional challenges with the proposed method are summarized as follows.

1) Computation burden: Different from the existing local control schemes, additional calculation time is required with the proposed real-time voltage regulation scheme in each control cycle. In order to keep up with fast fluctuations of PV power, the established optimization formulation should always be rapidly solved.

2) Communication time delay: The real-time measurements collected by different devices should be transmitted to a control centre as inputs of the proposed voltage regulation method. Then, commands obtained in the control centre should be sent back to corresponding devices at the end of each control cycle. Therefore, real-time communication between devices and the control centre is required, and the communication time delay needs to be considered in the proposed method.
3) Risk of communication outage: The optimization based method will be invalid when the communication system is accidently broken down. Therefore, all devices should be seamlessly transferred from the central control mode to the local control mode, if they do not receive any commands from the control centre for a certain period of time.

The real-time voltage regulation method which will be executed in each 5s control cycle is proposed in this paper. With established convex optimization problems, the solving time is around 0.4s. In addition, since both PV inverters and BESS are installed in the same platform in close vicinity of each other, the communication time delay is negligible. Therefore, the procedure of calculation and communication can always keep up with the 5s control cycle. Finally, both PV inverters and BESS have been designed to seamlessly transit to their original local control schemes during the communication system outage.

VII. Simulation Platforms

Currently, the University of Queensland is in the process of installing the Open Process Control (OPC) interface for the Gatton PV plant. This interface can enable programming of real-time plant control using MatLab, which is much simpler and more flexible than PLC programming. Through this OPC interface, bidirectional communication can be established between MatLab and the SCADA system. Consequently, PV inverters and BESS can be centrally coordinated and controlled by algorithms coded in MatLab located in a control centre. This control centre can read real-time field recorded measurements and write control commands every one second through the OPC interface.

Before the field application, the proposed method should be first verified by the laboratory experiment with a real time digital simulator. Therefore, the RTDS-MatLab co-simulation platform is established to validate the effectiveness of the developed coordination algorithm. In this platform, the actual system and the control centre are separately simulated by RTDS and MatLab algorithms respectively, and a bidirectional communication link is created between RTDS and MatLab. Details of this co-simulation platform is provided as follows.

A. Characteristics of RTDS

Different from pure computer based simulations, the RTDS has its own internal clock. If the external control command from MatLab cannot be obtained in time due to a complex calculation or a communication time delay or a communication outage, the RTDS will never stop its real-time simulation and wait for such a control command. Therefore, the RTDS can precisely simulate the behaviour of an actual power system in real time.

B. Platform Structure

As shown in Fig. 8 below, the hardware of RTDS is installed in the Frank White Building, which is used to simulate the studied distribution system (Fig. 1) and the PV plant (Fig. 2) in real time. While, the MatLab installed in the Computer I in the Axon Building will work as the control centre during simulations. The distance between these two buildings is around 100 meters. The established communication link between MatLab and the remote RTDS is based on the TCP socket communication program model, where the GTNETx2 card of the RTDS works as a remote socket server, and the MatLab program in Computer I is a socket client. Therefore, this RTDS-MatLab co-simulation platform is a close representation of the actual system, which includes the distribution network, PV-BESS system, PLC, SCADA, OPC interface and MatLab.

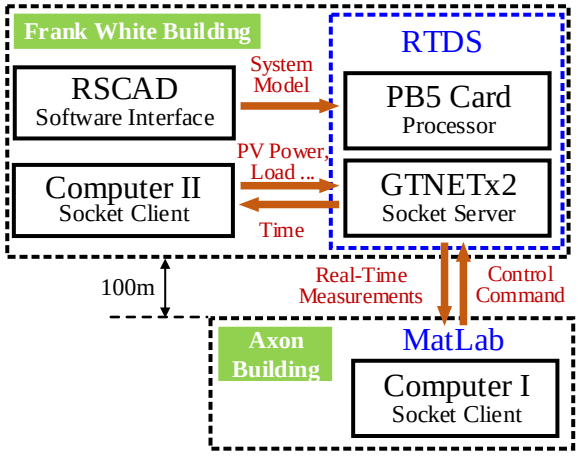

Fig. 8 Structure of RTDS-MatLab co-simulation platform.

C. Simulation Procedure

Before the simulation, the established Gatton distribution system model (including network and PV plant) should be uploaded to the RTDS through its software interface RSCAD. During the simulation, the RTDS conducts simulation in a 50μs time step, and load, upstream voltage and PV generation in the RTDS are updated every one second by Computer II (as in Fig. 8). The proposed algorithm (coded in MatLab) executed in Computer I only relies on the real-time measurements from RTDS in each control cycle. Then, the control commands generated from MatLab will be sent back to RTDS at the end of each control cycle.

The one-day results from the RTDS-MatLab co-simulation platform using field recorded data (1s resolution) are demonstrated in the next section to verify the effectiveness of the proposed method for the real-time application. The results show that with typical communication and calculation time delays, the reading, calculating and writing processes in the proposed method can always be completed within each control cycle (i.e. a 5-second period). Occasionally, a communication outage, which can be recovered within one or two seconds, does not have any significant impacts on the control performance. While, in case of a longer communication outage, PV inverters and BESS will be seamlessly switched from the central control mode to their original local control mode to ensure the continuity of voltage regulation.

VIII. Time Series Verification

To demonstrate the effectiveness and advantages of the proposed real-time coordinated voltage control strategy, field recorded PV generation and load data (1s resolution) on one typical day (30th January 2017) are utilized as simulation inputs for validation in this section. The upstream voltage profile in that day is shown in Fig. 9.

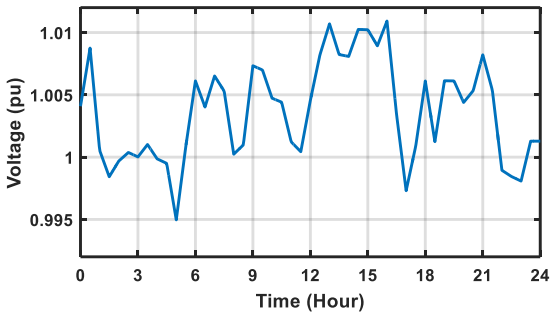

Fig. 9 Upstream voltage profile.

A. Challenges with Existing Local Voltage Regulation Schemes

As shown in Table I, on 30th January 2017 (a typical cloudy day), if the PV power is assumed to be zero (the Pre-PV integration scenario), the upstream SVR can successfully control the system voltage with 13 and 14 tap operations for SVR1 and SVR2, respectively. However, for the same network conditions with PV generation (existing PV inverter control scenario), the tap changes are 4 to 5 times more than the Pre-PV integration case.

TABLE I
SVR Tap Operations and Battery Charging/Discharging Energy

Scenarios	Processed Energy by BESS	Tap (SVR1)	Tap (SVR2)
Pre-PV Integration	Not Applicable	13	14
Existing PV Inverter Control	Not Applicable	67	58
5-min Moving Average	3625kWh	51	48
10-min Moving Average	5290kWh	41	32
20-min Moving Average	7053kWh	19	16
Proposed Method	556kWh	10	13

The installed 760kWh BESS can mitigate PV power fluctuations through its charging/discharging operations. Consequently, excessive SVR tap operations can be mitigated. As shown in Table I, with 10-minute moving average algorithm, the tap operations of SVR1 (SVR2) in one day reduces from 67 (58) times to 41 (32) times at a cost of processing 5290kWh charging/discharging energy by the BESS (around 7 times of its rated capacity). The tap operations of SVR1 and SVR2 can be further reduced to 19 and 16 times when the window length of the moving average algorithm is set to be 20-minute. However, the BESS will be overused with 7053kWh energy flow during that day.

In order to balance the voltage regulation performance and the related cost, 5-minute moving average algorithm is implemented in current PV plant operation. As shown in Fig. 10, frequently BESS charging/discharging operation can be observed, with 3625kWh total processed energy during one typical cloudy day (30th January 2017). However, with smoothed PV power, voltage violations still exist with an accumulative period of 234s as shown in Fig. 11 a). At the same time, tap operations of SVR1 and SVR2 are 51 and 48 times respectively during that day.

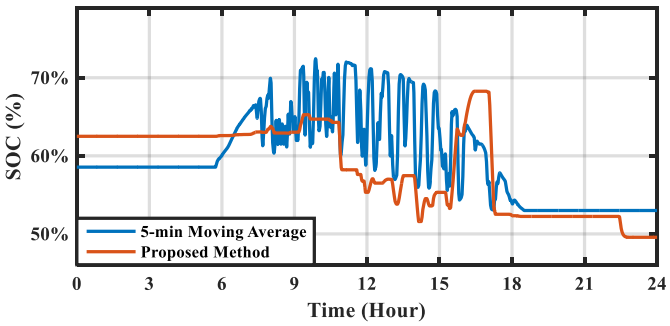

Fig. 10 SOC profiles with moving average and proposed control methods.

B. Proposed Voltage Control Method

Compared with the 5-minute moving average algorithm, the excessive charge/discharge of BESS can be significantly mitigated with the proposed method, as shown in Fig. 10. As a result, the total processed energy is reduced to 556kWh during one day. In addition, voltage violation risk can be removed in each 5s control cycle. Consequently, no voltage violation occurs during this day as shown in Fig. 11 b). Furthermore, only 10 and 13 tap operations of SVR1 and SVR2 are triggered, which is comparable to the situation before the integration of the PV plant, as shown in Table I.

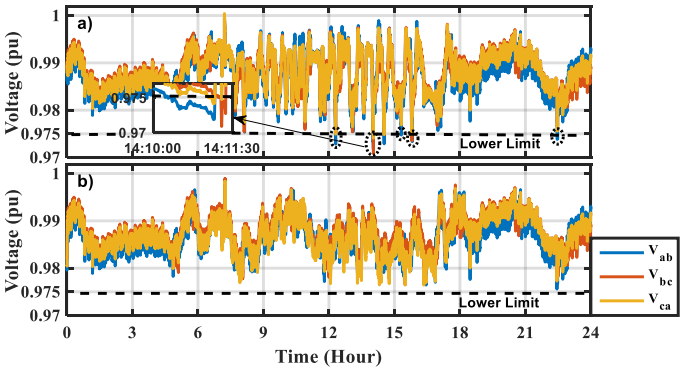

Fig. 11 Voltage profile at PCC a) with existing method; b) with proposed control method.

As designed in the proposed method, reactive power always has a priority for voltage compensation in each control cycle. BESS will be used only when PV inverters have reached their power factor limits. As shown in the zoom-in picture of Fig. 12, PV generation experiences a continuous decrease from 10:48:20 as a result of cloud coverage. At the same time, reactive power injection from PV inverters correspondingly increases to counter the voltage variation caused by PV power drop. However, after 10:50:30, reactive power injection cannot increase further due to power factor restriction, and it begins to drop with the reduction of PV active power at a constant power factor of 0.9. At this instant, active power output from BESS starts to join in the voltage regulation. The active power support from BESS lasts around 7 minutes 10 seconds during this period. After PV power rises again, the active power output of BESS gradually reduces back to zero to mitigate the pressure on BESS.

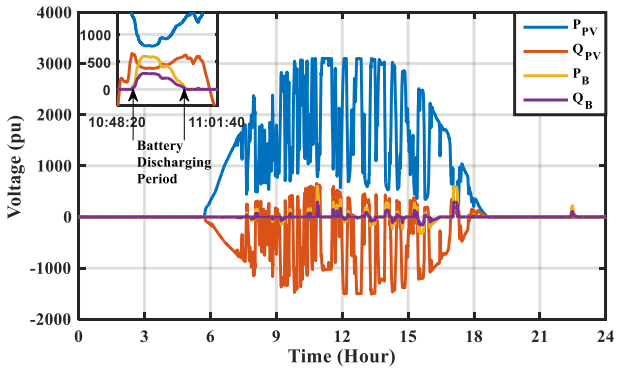

Fig. 12 Q_{PV} from PV inverters and P_B and Q_B from battery inverters.

C. BESS Premature Exhaustion without SOC Regulation

Without the active adjustment method for SOC regulation, the operation of PV inverters and BESS will only follow the results of the optimization algorithm. As previously discussed, the optimization algorithm only focuses on the optimal voltage regulation in each control cycle (a 5-second period). Consequently, SOC may easily reach its upper or lower limits due to lack of long-term management strategy. Fig. 13 demonstrates the one-day SOC profile with load and PV data recorded on 30th January 2017 (same data are used by the proposed method in Part B of this section). However, without active adjustment method for SOC regulation, the SOC of BESS reaches its lower limit in the afternoon, as shown in Fig. 13. During such periods, the system becomes vulnerable to voltage violations because the BESS may be unavailable for voltage regulation. For example, as in Fig. 14, the PCC voltage violates its lower limit around 3:45pm when SOC reaches its lower limit as in Fig. 13.

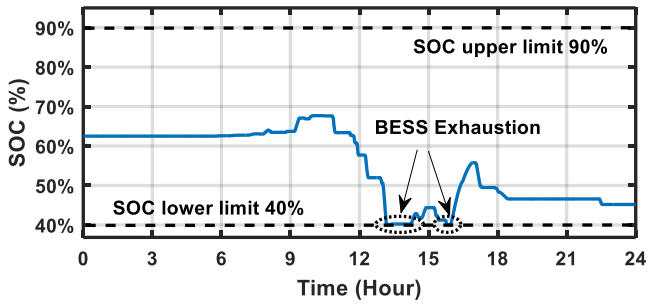

Fig. 13 SOC profile without active adjustment method.

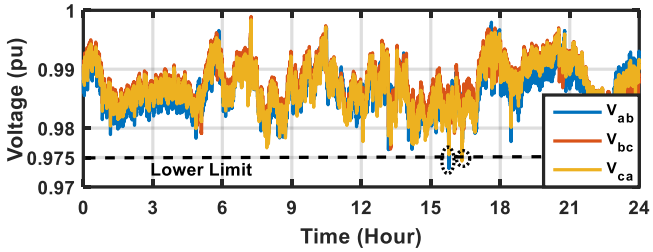

Fig. 14 PCC Voltage without active adjustment method.

IX. Conclusions

An innovative real-time coordinated control scheme is proposed in this paper for voltage regulation in weak distribution systems with high PV penetration. It makes use of reactive power of PV and BESS inverters as a priority and is coordinated with active power output of BESS in each 5s control cycle considering practical limits of a real-life application (e.g. BESS size, ramp rate, power factor ranges, etc). Further, control parameters of PV inverters and BESS are systematically designed to achieve automatic coordination with upstream SVR. This approach guarantees that PV inverters and BESS are mainly used to deal with fast fluctuations of PV power output, while SVR is responsible for voltage variations caused by slow load changes. In addition, active adjustment of BESS charging/discharging power is developed to ensure the SOC of BESS will not reach its upper or lower limit within an unacceptable time.

The effectiveness of the proposed approach is demonstrated with one typical day field recorded data. The results show that voltage violations at PCC are considerably mitigated. Moreover, the total processed energy of BESS are significantly reduced, and only a reasonable number of SVR tap operations are required every day, which is comparable to the situation of pre-integration of the large-scale PV plant. In summary, this paper provides valuable experience for voltage regulation in weak systems with high PV penetration, which can help to facilitate future integration of large PV plants into rural areas.

X. Appendices

A. SVR with Open-Delta Connection

Step Voltage Regulator (SVR) is originally designed to compensate slowly changing voltage through switching its tap positions. For the Gatton distribution system, an SVR with open-delta connection is installed in the middle of the feeder which is responsible for downstream voltage regulation before the integration of the 3.275MW PV plant.

As shown in Fig. A1 a), two single phase SVRs are connected between phases A and B (SVR1) as well as phases C and B (SVR2). The line drop compensation (LDC) scheme [26] is applied on each one-phase SVR for remote voltage estimation. For example, SVR1 measures the line-to-line (phase A-B) voltage $V_{AB,sec}$ at its secondary side and line current I_A at phase A to estimate remote line-to-line voltage as

$$V_{AB,est} = V_{AB,sec} - I_A(R + jX) \quad \text{(A1)}$$

where $V_{AB,est}$ represents the estimated remote line-to-line voltage; $R + jX$ represents the equivalent line parameters. The LDC parameter setting rule for SVR with open-delta connection is in [27]. When remotely estimated voltage $V_{AB,est}$ is lower than $V_t - \Delta V_{db}$ (V_t and ΔV_{db} represent the voltage target and dead band respectively), the SVR begins to count the low voltage time. SVR will change its tap position to correct voltage if this low voltage lasts longer than SVR time delay T_d. Similar tap operation will be done in situations when a high voltage ($> V_t + \Delta V_{db}$) lasts longer than the SVR time delay. Please refer to [26] for more details on SVR tap switching mechanism. In this paper, V_t, ΔV_{db} and T_d are set to be 0.9875pu, 0.00625pu, 135s respectively, which are real settings obtained from the local utility. Parameters of the SVR control logic are shown in Table A1.

With the open-delta connected SVR, the downstream line-to-line voltage variation can be compensated by SVR tap operations, as shown in Fig. A1 b). The campus load is

fed through 11kV/415V transformers with delta-grounded wye connection. Consequently, phase voltages of the 415V side can be controlled as long as line-to-line voltages at the 11kV side can always be properly regulated.

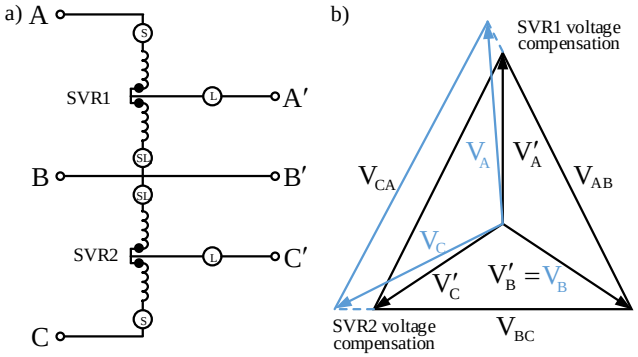

Fig. A1 a) SVR structure with open-delta connection [26, 28], b) voltage vectors of primary and secondary side of SVRs.

TABLE A1
SVR CONTROL PARAMETERS

	SVR1 (between Phase A and B)	SVR2 (between Phase C and B)
LDC parameters	0.139+j0.768 Ω	0.735+j0.264 Ω
Time Delay	135s	135s
Voltage Target	0.9875pu	0.9875pu
Dead Band	0.00625pu	0.00625pu

B. Power Factor Droop Curve

Currently, the local reactive power compensation method following the predefined power factor droop curve [20] is implemented on PV inverters for voltage regulation. As shown in Fig. B1, the power factor of PV inverters will vary within the allowable range (0.9 lagging to 0.9 leading) according to the measured local voltage. For example, if the local voltage is too high, PV inverters will operate at an inductive power factor to absorb reactive power from the distribution system, and vice versa. Currently, four parameters V_{low}, V_{m1}, V_{m2} and V_{high} are set to be 0.97pu, 0.98pu, 0.992pu and 1.002pu respectively.

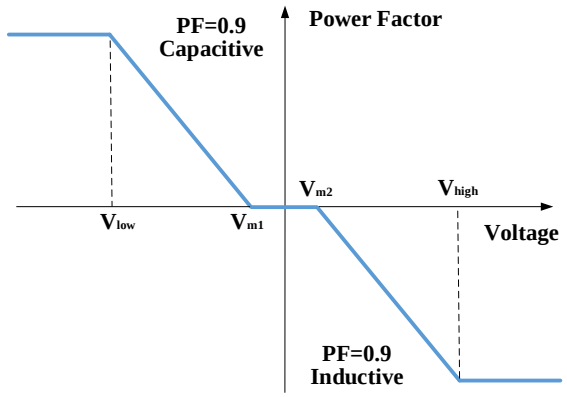

Fig. B1 Power factor droop curve.

C. Moving Average Algorithm

A 760kWh BESS is installed in the Gatton PV plant for PV power smoothing with a moving average algorithm [13]. In this method, the average PV generation $\overline{P_{PV}}(t)$ of a past period T is calculated as

$$\overline{P_{PV}}(t) = \frac{1}{T}\int_{t-T}^{t} P_{PV}(t)\,dt \quad \text{(C1)}$$

where $P_{PV}(t)$ represents the PV plant generation at time instant t; T is the time window length. Correspondingly, the battery storage output $P_B(t)$ is expressed as

$$P_B(t) = \overline{P_{PV}}(t) - P_{PV}(t) + k \cdot (SOC(t) - SOC_{mid}) \quad \text{(C2)}$$

where $SOC(t)$ represents the state of charge of the BESS at time instant t; SOC_{mid} represents the middle level of SOC of the BESS. k is the weight factor, which is used to prevent SOC from leaving its middle level too far away. It is worth noting, if a larger T and a smaller k are selected, a better power smoothing effect can be obtained at a cost of requiring more charging/discharging energy of the BESS. Conversely, if a smaller T and a larger k are selected, less charging/discharging energy will be processed by the BESS resulting in lower power smoothing performance.

D. Proof for the Active Adjustment Method

Proof is provided as below to show that the designed active adjustment method can realize the SOC regulation functionalities as presented in Section V Part A.

Proof 1 (Direction of Adjustment):

According to (17), a positive ΔP_B obtained from the optimization algorithm will be retuned to ΔP_B^m as below

$$\Delta P_B^m = \Delta P_B e^{\frac{c_2(SOC - SOC_{mid})}{SOC - SOC_{min}}} \quad \text{(D1)}$$

Let $f_p(SOC) = \frac{c_2(SOC - SOC_{mid})}{SOC - SOC_{min}}, SOC \in (SOC_{min}, SOC_{max})$

$$\dot{f_p}(SOC) = \frac{c_2(SOC_{mid} - SOC_{min})}{(SOC - SOC_{min})^2} > 0 \quad \text{(D2)}$$

Therefore, $f_p(SOC)$ is monotonically increasing. Further, since both $f_p(SOC)$ and e^x are monotonically increasing functions, $\Delta P_B^m = e^{f_p(SOC)}$ is also a monotonically increasing function.

$$\therefore ① \ \Delta P_B^m > \Delta P_B \ if \ SOC > SOC_{mid}$$
$$\text{and } \Delta P_B^m < \Delta P_B \ if \ SOC < SOC_{mid}$$

In addition, for a positive ΔP_B, we can obtain

$$SOC \to SOC^{+}_{min} \Rightarrow f_p(SOC) \to -\infty$$
$$\Rightarrow e^{f_p(SOC)} \to 0^+ \Rightarrow \Delta P_B^m \to 0^+ \quad \text{(D3)}$$
$$\therefore ② \ SOC \to SOC^{+}_{min} \Rightarrow \Delta P_B^m \to 0^+$$

Similarly, for a negative ΔP_B, we can obtain $SOC \to SOC^{-}_{max} \Rightarrow \Delta P_B^m \to 0^-$.

The functionalities of Direction of Adjustment are proved. ■

Proof 2 (Magnitude of Adjustment):

The magnitude of the active adjustment equals to the absolute difference between ΔP_B and ΔP_B^m. Let $g_p(SOC) = |\Delta P_B^m - \Delta P_B|$ if the obtained ΔP_B is positive, therefore

$$g_p(SOC) = \left|\Delta P_B\left(e^{f_p(SOC)} - 1\right)\right| = \Delta P_B\left|e^{f_p(SOC)} - 1\right| \quad \text{(D4)}$$

Since $e^{f_p(SOC)} - 1$ is a monotonically increasing function and $g_p(SOC_{mid}) = 0$, we can obtain

$$g_p(SOC)\begin{cases}\text{monotonically increases}, SOC > SOC_{mid}\\ \text{monotonically decreases}, SOC < SOC_{mid}\end{cases} \quad \text{(D5)}$$

Namely,

$$\therefore ③\ |\Delta P_B^m - \Delta P_B|\begin{cases}\text{monotonically increases}, SOC > SOC_{mid}\\ \text{monotonically decreases}, SOC < SOC_{mid}\end{cases}$$

In addition, $g_p(SOC)$ is continuous in the neighbourhood of $SOC = SOC_{mid}$.

$$\therefore ④\ SOC \to SOC_{mid} \Rightarrow \Delta P_B^m \to \Delta P_B$$

Same conclusion can be made with the situation when a negative ΔP_B is obtained from the optimization algorithm.

The functionalities of Magnitude of Adjustment are proved. ■

E. System Parameters

TABLE E1
THREE-PHASE LINE PARAMETERS

Type	(R+jX) in ohms per kilometre		
Moon	0.33+j0.76	0.049+j0.424	0.049+j0.39
	0.33+j0.76	0.049+j0.42	
		0.33+j0.76	
UG	0.12+j0.079	0.038-j0.013	0.038-j0.013
	0.121+j0.079	0.038-j0.013	
		0.121+j0.079	

TABLE E2
PARAMETERS OF THE DISTRIBUTION TRANSFORMER

	Rated Voltage	Connection	X	R
Winding1	11kV	Delta	4.93%	0.84%
Winding2	433V	Grounded-Wye		

TABLE E3
PARAMETERS OF PV ARRAYS [20]

Each PV array	Number of arrays	DC rating	AC rating	Reactive power ramp rate
7,200 First Solar 95 W Series 3 CdTe PV panels and one SMA SC720CP inverter	5	684kW	720kVA	10kVar/s

TABLE E4
PARAMETERS OF BESS [29]

Inverter type	DC rating	AC rating	Active power ramp rate	Reactive power ramp rate
SMA SC720CP	600kW	720kVA	10kW/s	10kVar/s

XI. REFERENCES

[1] S. Alyami, Y. Wang, C. S. Wang, J. H. Zhao, and B. Zhao, "Adaptive Real Power Capping Method for Fair Overvoltage Regulation of Distribution Networks With High Penetration of PV Systems," *IEEE Transactions on Smart Grid*, vol. 5, pp. 2729-2738, Nov 2014.

[2] F. Olivier, P. Aristidou, D. Ernst, and T. Van Cutsem, "Active Management of Low-Voltage Networks for Mitigating Overvoltages Due to Photovoltaic Units," *IEEE Transactions on Smart Grid*, vol. 7, pp. 926-936, Mar 2016.

[3] M. I. Hossain, R. Yan, and T. K. Saha, "Investigation of the interaction between step voltage regulators and large-scale photovoltaic systems regarding voltage regulation and unbalance," *IET Renewable Power Generation*, vol. 10, pp. 299-309, 2016.

[4] S. Abulanwar, W. Hu, F. Iov, and Z. Chen, "Adaptive voltage control strategy for variable-speed wind turbine connected to a weak network," *IET Renewable Power Generation*, vol. 10, pp. 238-249, 2016.

[5] E. Bullich-Massagué, O. Gomis-Bellmunt, L. Serrano-Salamanca, R. Ferrer-San-José, C. Pacheco-Navas, and M. Aragüés-Peñalba, "Power plant control in large-scale photovoltaic plants: design, implementation and validation in a 9.4 MW photovoltaic plant," *IET Renewable Power Generation*, vol. 10, pp. 50-62, 2016.

[6] S. Deshmukh, B. Natarajan, and A. Pahwa, "Voltage/VAR Control in Distribution Networks via Reactive Power Injection Through Distributed Generators," *IEEE Transactions on Smart Grid*, vol. 3, pp. 1226-1234, Sep 2012.

[7] B. A. Robbins, C. N. Hadjicostis, and A. D. Dominguez-Garcia, "A Two-Stage Distributed Architecture for Voltage Control in Power Distribution Systems," *IEEE Transactions on Power Systems*, vol. 28, pp. 1470-1482, May 2013.

[8] L. Wang, R. Yan, and T. K. Saha, "Voltage Management for Large Scale PV Integration into Weak Distribution Systems," *IEEE Transactions on Smart Grid*, 2017.

[9] Energex Limited (Energex) and The University of Queensland (Customer). (2011). "Negotiated Customer Connection Contract (without construction, with generator embedded within customer network)." Available: https://www.gci.uq.edu.au/filething/get/6363/NCC-without-Construction-with-Generator-Embedded_v5_Executed%20201114-Technical%20Extract-8.pdf

[10] M. Zeraati, M. E. Hamedani Golshan, and J. Guerrero, "Distributed Control of Battery Energy Storage Systems for Voltage Regulation in Distribution Networks with High PV Penetration," *IEEE Transactions on Smart Grid*, DOI 10.1109/TSG.2016.2636217.

[11] X. Liu, A. Aichhorn, L. Liu, and H. Li, "Coordinated Control of Distributed Energy Storage System With Tap Changer Transformers for Voltage Rise Mitigation Under High Photovoltaic Penetration," *IEEE Transactions on Smart Grid*, vol. 3, pp. 897-906, 2012.

[12] M. J. E. Alam, K. M. Muttaqi, and D. Sutanto, "Effective Utilization of Available PEV Battery Capacity for Mitigation of Solar PV Impact and Grid Support With Integrated V2G Functionality," *IEEE Transactions on Smart Grid*, vol. 7, pp. 1562-1571, 2016.

[13] N. Kakimoto, H. Satoh, S. Takayama, and K. Nakamura, "Ramp-Rate Control of Photovoltaic Generator With Electric Double-Layer Capacitor," *IEEE Transactions on Energy Conversion*, vol. 24, pp. 465-473, 2009.

[14] Z. Tang, D. Hill, T. Liu, and H. Ma, "Hierarchical Voltage Control of Weak Subtransmission Networks with High Penetration of Wind Power," *IEEE Transactions on Power Systems*, vol. 33, pp. 187-197, 2018.

[15] N. Daratha, B. Das, and J. Sharma, "Coordination Between OLTC and SVC for Voltage Regulation in Unbalanced Distribution System Distributed Generation," *IEEE Transactions on Power Systems*, vol. 29, pp. 289-299, Jan 2014.

[16] Z. Y. Wang, H. Chen, J. H. Wang, and M. Begovic, "Inverter-Less Hybrid Voltage/Var Control for Distribution Circuits With Photovoltaic Generators," *IEEE Transactions on Smart Grid*, vol. 5, pp. 2718-2728, Nov 2014.

[17] S. W. Alnaser and L. F. Ochoa, "Advanced Network Management Systems: A Risk-Based AC OPF Approach," *IEEE Transactions on Power Systems*, vol. 30, pp. 409-418, 2015.

[18] X. J. Su, M. A. S. Masoum, and P. J. Wolfs, "Multi-Objective Hierarchical Control of Unbalanced Distribution Networks to Accommodate More Renewable Connections in the Smart Grid Era," *IEEE Transactions on Power Systems*, vol. 31, pp. 3924-3936, Sep 2016.

[19] RTDS. Available: https://www.rtds.com/

[20] V. Garrone, M. Hibbert, J. Mayer, "Technical Requirements for the Connection of a MW-scale PV Array with Battery Storage to an 11kV Feeder in Queensland," *Asia-Pacific Solar Research Conf.*, 2014.

[21] H. Farzin, M. Fotuhi-Firuzabad, and M. Moeini-Aghtaie, "A Practical Scheme to Involve Degradation Cost of Lithium-Ion Batteries in Vehicle-to-Grid Applications," *IEEE Transactions on Sustainable Energy*, vol. 7, pp. 1730-1738, 2016.

[22] A. D. Orjuela-Cañón, J. Hernández, and C. R. Rivero, "Very short term forecasting in global solar irradiance using linear and nonlinear models," Bogota, Colombia 2017.

[23] CVX. Available: http://cvxr.com/cvx/

[24] A. Samadi, R. Eriksson, L. Soder, B. G. Rawn, and J. C. Boemer, "Coordinated Active Power-Dependent Voltage Regulation in Distribution Grids With PV Systems," *IEEE Transactions on Power Delivery*, vol. 29, pp. 1454-1464, Jun 2014.

[25] V. Calderaro, G. Conio, V. Galdi, G. Massa, and A. Piccolo, "Optimal Decentralized Voltage Control for Distribution Systems With Inverter-Based Distributed Generators," *IEEE Transactions on Power Systems*, vol. 29, pp. 230-241, 2014.

[26] W. H. Kersting, *Distribution System Modelling and Analysis*: CRC Press, 2002.

[27] Cooper Power Systems, "Determination of Regulator Compensator Settings," R225-10-1, 2003.

[28] R. Yan, Y. Li, T. Saha, L. Wang, and M. Hossain, "Modelling and Analysis of Open-Delta Step Voltage Regulators for Unbalanced Distribution Network with Photovoltaic Power Generation," *IEEE Transactions on Smart Grid*, DOI: 10.1109/TSG.2016.2609440.
[29] M. J. E. ALAM, R. YAN, T. K. SAHA, A. CHIDURALA, and D. EGHBAL, "Learning from a 3.275 MW Utility Scale PV Plant Project," CIGRE, Paris, 2016.

Licheng Wang (S'2016) completed his B.Sc from Huazhong University of Science and Technology in 2012, and completed his M.Sc from Zhejiang University in 2015. Currently, he is a PhD student in the Power & Energy Systems Research Division at the School of Information Technology and Electrical Engineering, the University of Queensland, Australia. His research interest is renewable energy integration into distribution systems.

Feifei Bai (S'13, M'16) received the B.S. degree and Ph.D. degree in Power System and Automation from Southwest Jiaotong University, China, in 2010 and 2016, respectively. She was a joint-Ph.D. student at the University of Tennessee, Knoxville, USA, from 2012 to 2014. She is currently a postdoctoral research fellow in the School of Information Technology and Electrical Engineering, University of Queensland, Australia. Her main research interests are renewable energy integration into power grid, small signal stability analysis and wide-area damping control.

Ruifeng Yan (S'2009, M'2012) received the B. Eng. (Hons.) degree in Automation from University of Science and Technology, Beijing, China, in 2004, the M. Eng degree in Electrical Engineering from the Australian National University, Canberra, Australia, in 2007, and Ph.D. degree in Power and Energy Systems from the University of Queensland, Brisbane, Australia, in 2012. He won the Discovery Early Career Researcher Award (DECRA) from Australia Research Council (ARC) in 2017. His research interests include power system operation and analysis, and renewable energy integration into power networks.

Tapan Kumar Saha (M'93, SM'97) was born in Bangladesh in 1959 and immigrated to Australia in 1989. He received his B. Sc. Engineering (electrical and electronic) in 1982 from the Bangladesh University of Engineering & Technology, Dhaka, Bangladesh, M. Tech (electrical engineering) in1985 from the Indian Institute of Technology, New Delhi, India and PhD in 1994 from the University of Queensland, Brisbane, Australia. Tapan is currently Professor of Electrical Engineering in the School of Information Technology and Electrical Engineering, University of Queensland, Australia. Previously he has had visiting appointments for a semester at both the Royal Institute of Technology (KTH), Stockholm, Sweden and at the University of Newcastle (Australia). He is a Fellow of the Institution of Engineers, Australia. His research interests include condition monitoring of electrical plants, power systems and power quality.